Journal of Medicinal Chemistry

Article

Molecular Dynamics Simulations of the Endocannabinoid *N*-Arachidonoylethanolamine (Anandamide) in a Phospholipid Bilayer: Probing Structure and Dynamics

Diane L. Lynch, and Patricia H. Reggio

J. Med. Chem., **2005**, 48 (15), 4824-4833• DOI: 10.1021/jm058185d • Publication Date (Web): 01 July 2005

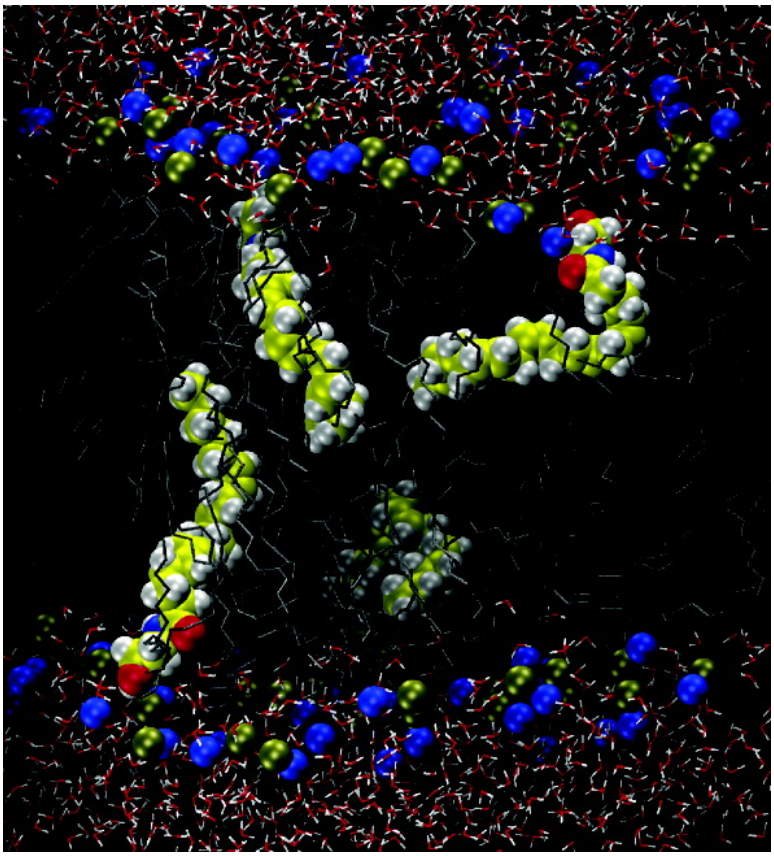

More About This Article

Additional resources and features associated with this article are available within the HTML version:

- Supporting Information

Journal of Medicinal Chemistry is published by the American Chemical Society. 1155 Sixteenth Street N.W., Washington, DC 20036

Molecular Dynamics Simulations of the Endocannabinoid *N*-Arachidonoylethanolamine (Anandamide) in a Phospholipid Bilayer: Probing Structure and Dynamics

Diane L. Lynch[†] and Patricia H. Reggio*[,‡]

Department of Chemistry and Biochemistry, Kennesaw State University, Kennesaw, Georgia 30144-5591, and Department of Chemistry and Biochemistry, University of North Carolina Greensboro, Greensboro, North Carolina 27402-6170

Received February 3, 2005

The phospholipid bilayer plays a central role in the lifecycle of the endogenous cannabinoid *N*-arachidonoylethanolamine (anandamide, **1**). Compound **1** has been shown to be synthesized from lipids, to interact with the membrane-embedded cannabinoid CB1 receptor, to be transported to intracellular compartments, possibly via caveolae-related endocytosis, and finally, to be degraded by fatty acid amide hydrolase (FAAH), an integral membrane protein which has an active site that is accessed by **1** possibly via the bilayer. Because the anandamide system is intimately associated with the lipid milieu, information concerning the location of **1** in the phospholipid bilayer and the conformations it can adopt is important to our understanding of the mechanism of cannabinoid action at the molecular level. We report here an exploration of the properties of **1** in a 1,2-dioleoyl-*sn*-glycero-3-phosphocholine (DOPC) phospholipid bilayer via multi-nanosecond molecular dynamics simulations. Our results suggest that the polar headgroup of **1** resides at the lipid−water interface, specifically in the polar phospholipid headgroup region, whereas the nonpolar acyl chain of **1** extends into the hydrocarbon core of the membrane. Our analysis also indicates that (i) an elongated conformation of **1** is preferred in the DOPC bilayer environment; however, many other conformations of **1** are observed; (ii) hydrogen-bonding between the lipid (DOPC) and the headgroup of **1**, although extensive, is quite short-lived; and (iii) the C−H bond order parameters for the acyl chain of **1** are low compared to order parameters typically seen for saturated acyl chains of fatty acids, and these order parameters decrease toward the bilayer center. The bilayer location for **1** revealed by these studies may be important for the interaction of **1** with membrane-embedded proteins such as the cannabinoid CB1 receptor and membrane-associated proteins such as FAAH.

Work to date on the cannabinoid system has indicated that it is intimately related to the lipid milieu. The endogenous ligands for the cannabinoid CB1 receptor, including *N*-arachidonoylethanolamine (anandamide **1**, see Chart 1),[1] *sn*-2-arachidonoylglycerol (2AG),[2] and 2-arachidonyl glyceryl ether,[3] are highly lipophilic, lipid-derived molecules. The endocannabinoid system has been proposed to mediate the suppression of GABA release from presynaptic terminals following the depolarization of a hippocampal CA1 pyramidal neuron. This process is termed the depolarization-induced suppression of inhibition (DSI).[4] In DSI, **1** has been shown to serve as a retrograde signaling molecule. Compound **1** can be rapidly synthesized postsynaptically from lipids by neurons in response to depolarization and a consequent Ca^{2+} influx.[5,6] It is not yet clear for retrograde signaling how newly synthesized **1** is induced to leave the postsynaptic plasma membrane to interact with the G protein-coupled cannabinoid CB1 receptor, which is located presynaptically. Compound **1** may be secreted by simple diffusion; alternatively, passive (energy-independent) carrier proteins may be required to extrude **1**.[6,7] The subsequent activation of CB1 by **1** results in the inhibition of Ca^{2+} channels in the presynaptic cell. Following CB1 activation, **1** is transported into the intracellular compartment of the postsynaptic cell by either a carrier-mediated[7−9] or a simple diffusion process.[10] Cellular uptake may also be facilitated by caveolae/lipid raft-related endocytosis.[11] Compound **1** is rapidly metabolized by a membrane-associated enzyme, fatty acid amide hydrolase (FAAH), which is located in the endoplasmic reticulum and has an active site that is accessed by **1** possibly via the bilayer.[12] Clearly, the phospholipid bilayer plays a central role in the lifecycle of **1**. Therefore, the location of **1** in the phospholipid

Chart 1. Chemical Structures of **1** and DOPC

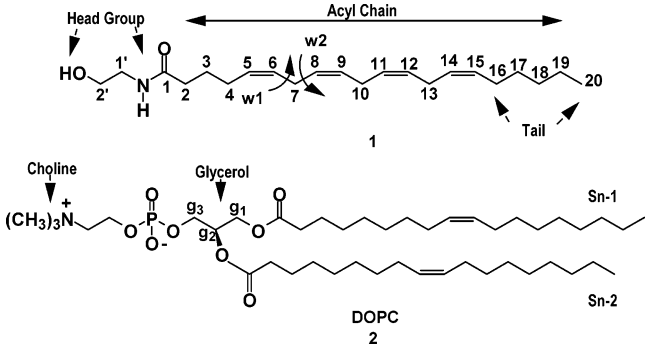

* Address correspondence to this author at Department of Chemistry and Biochemistry, University of North Carolina Greensboro, P.O. Box 26170, 435 New Science Building, Greensboro, NC 27402-6170. Phone: (336) 334-5333. Fax: (336) 334-5402. E-mail: phreggio@uncg.edu.

[†] Kennesaw State University.

[‡] University of North Carolina Greensboro.

10.1021/jm058185d CCC: $30.25
Published on Web 07/01/2005

bilayer, as well as its orientation with respect to key membrane-associated proteins, is a central issue in understanding the mechanism of such lipid-based signaling events at the atomic level.

Earlier molecular dynamics (MD) and Monte Carlo (MC)-based studies have explored the conformational preferences of the endocannabinoid **1** in various environments. For example, Thomas and co-workers[13] and Tong and co-workers[14] performed constrained MD calculations in a vacuum, while Piomelli and co-workers[8] performed MC calculations in a vacuum. Earlier MC/simulated annealing work from our laboratory[15,16] utilized an implicit solvent model for nonpolar ($CHCl_3$) or polar (water) environments. In addition, Bonechi and co-workers[17] have employed an MC scheme to study the conformational preferences of **1** using constraints derived from solution [dimethyl sulfoxide (DMSO)-d_6] NMR data. Given the amphipathic nature of **1**, its relative location and dynamics in lipids are expected to be strongly influenced by the presence of the polar phospholipid headgroup region and the hydrophobic core of the bilayer. To date, no endocannabinoid computational studies have been reported that contain an explicit inclusion of a hydrated phospholipid bilayer environment with its aqueous layer, chemically heterogeneous polar headgroup region, and hydrophobic core.

In the work reported here, we explore the structure, location, and dynamics of **1** in a model phospholipid bilayer via multi-nanosecond MD. We have used a fully hydrated bilayer of 1,2-dioleoyl-*sn*-glycero-3-phosphocholine (DOPC, see Chart 1) as our model membrane. The choice of DOPC was motivated primarily by the large body of computational and experimental data to which we could benchmark our pure bilayer results[18−22] and by the fact that DOPC is a constituent of brain phospholipids. Such calculations are complementary to experimental NMR studies currently in progress in other laboratories, which explore the location and dynamics of **1** in micelles or a phospholipid bilayer.[23,24]

Results

The two 5-ns MD trajectories for **1** in DOPC were analyzed to determine the structural and dynamical properties of **1** in DOPC. Analysis of these trajectories characterized: (i) the location in the lipid bilayer of the polar headgroup of **1**, as well as the terminal methyl group of **1**; (ii) the inter- and intramolecular hydrogen-bonding patterns of the polar headgroup of **1**; (iii) conformational distributions of the acyl chain of **1**; and (iv) order parameters for the C−H bonds in the acyl chain of **1**. To improve statistics in our MD runs for **1** in DOPC, four molecules of **1** were included in the high-hydration bilayer patch of DOPC reported here. The four molecules of **1** were placed apart from one another at distances that exceeded the 10-Å cutoff for nonbonded, short-range interactions employed in the calculations. For molecules of **1** in the same leaflet (averaged over the two 5-ns trajectories), the average distance between the hydroxyl oxygens was 27.5 Å. For molecules of **1** in different leaflets, also averaged over the trajectories, the average distance between the hydroxyl oxygens was 32.5 Å. Consequently, the molecules of **1** are far enough apart from each other during the simulation that they act independently of one another. In Figure 1, a snapshot is presented that was taken from the simulation, indicating a typical distribution of the molecular species in the calculation. The chemical structures of **1** and DOPC , as well as the numbering/labeling scheme and chemical composition of the various functional groups to be discussed below, are presented in Chart 1.

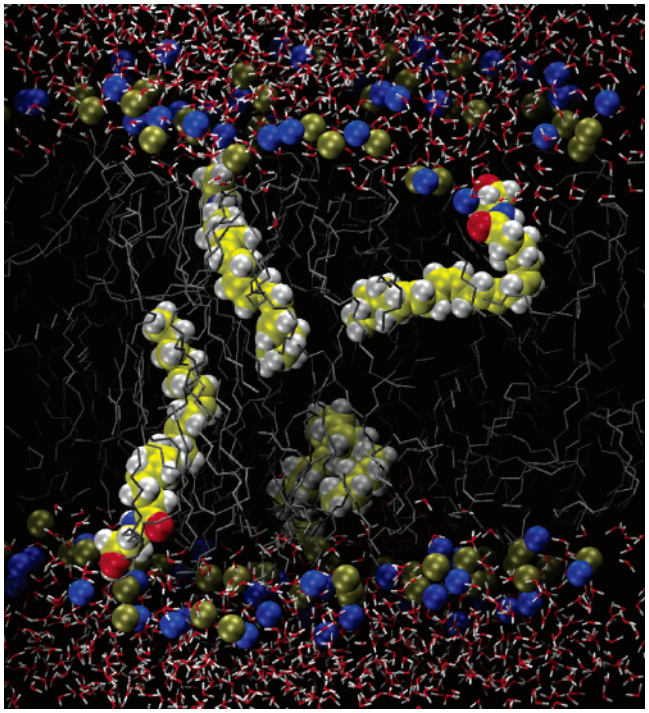

Figure 1. A simulation cell containing four molecules of **1**, DOPC, and water. A blue sphere represents the DOPC choline group nitrogen atom, and a gold sphere represents the DOPC phosphate group phosphorus atom. The DOPC acyl chains are shown in tube display and colored gray. Molecules of **1** are contoured at their van der Waals radii, with carbon atoms colored yellow; water is depicted here in tube display.

Group Distributions. The location of the polar headgroup of **1** in the DOPC bilayer was determined from the calculated trajectories. Once the *z*-direction was taken as normal to the plane of the membrane, group distributions were obtained by slicing along this direction and counting the number of heavy atoms in each functional group in each slice. To obtain a smooth graph, 200 slices were used. This produces a density per unit volume as a function of *z* for each time step in the simulation. These distributions were then averaged over the course of the MD simulation and scaled to the number of DOPC molecules (or molecules of **1**) in the simulation cell. The resultant group distribution for water (white) and the various DOPC moieties [phosphate (magenta), choline (cyan), glycerol (green), terminal methyl (red), and hydrophobic core (purple)] are illustrated in Figure 2a. It is clear here that water penetrates the polar headgroup region of the DOPC bilayer. This extent of water penetration has been noted for other lipid bilayers, such as 1-stearoyl-2-docosahexaenoyl-*sn*-glycero-3-phosphocholine (SDPC, 18:0/22:6 PC).[25] Chiu and co-workers found that the relatively horizontal orientation of the unsaturated bond in DOPC increases the area per lipid, resulting in an increase in water penetration between the headgroups. [21]

Scaled group distributions of the headgroup $-CH_2$-OH (yellow) and terminal methyl (orange) of **1** with

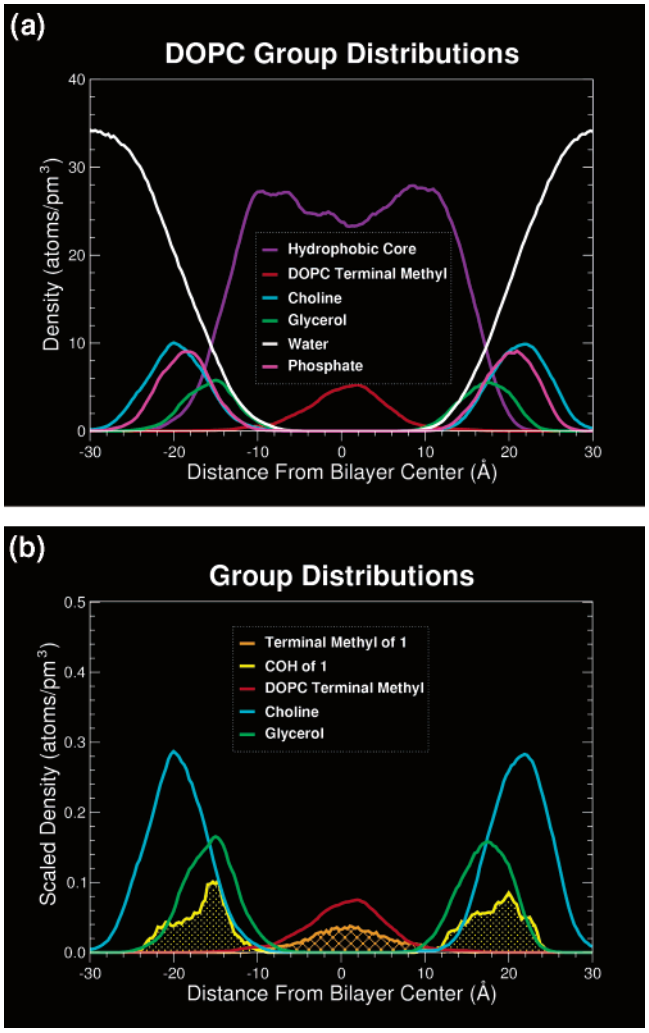

Figure 2. (a) Group distributions for water (white) and the various DOPC moieties, phosphate (magenta), choline (cyan), glycerol (green), terminal methyl (red), and hydrophobic core (purple). It is clear here that water penetrates into the polar headgroup region of the DOPC bilayer. (b) Scaled group distributions of the headgroup $-CH_2OH$ and terminal methyl of **1** with various DOPC moieties (choline, glycerol, and terminal methyl). Densities are scaled to the number of molecules. Here it is clear that the headgroup $-CH_2OH$ (yellow scored area) of **1** overlaps the glycerol (green) and choline (cyan) moieties of the DOPC phospholipid bilayer, being centered on the glycerol group. These results indicate that, on average, the headgroup hydroxyl of **1** resides in the DOPC headgroup region of the bilayer. This figure also shows the group distributions for the hydrocarbon tail (terminal methyl) of **1** (shown in orange hatched area) and the terminal methyl of DOPC (shown in red). It is clear here that the terminal methyl of **1** is embedded in the DOPC hydrocarbon core chain region of the bilayer with its maximum density at the bilayer center.

various DOPC moieties [choline (cyan), glycerol (green), and terminal methyl group (red)] are illustrated in Figure 2b. Densities are scaled to the number of molecules. Here, it is clear that the headgroup $-CH_2OH$ of **1** overlaps the glycerol and choline moieties of the DOPC phospholipid bilayer, being centered on the glycerol group. Moreover, the terminal methyl group of the DOPC (red in Figure 2b) lies in the center of the bilayer and does not significantly overlap the $-CH_2OH$ group of **1** (yellow scored area). These results indicate that, on average, the hydroxyl headgroup of **1** resides in the DOPC headgroup region of the bilayer. Because water penetrates this DOPC headgroup region (Figure 2a), it can also be said that the headgroup of **1** is located at the lipid/water interface.

Table 1. Average Energies of Interaction (E_{int}) in kcal/mol between the $C_{2'}$ Methylene Group[a] of **1** and Various DOPC Functional Groups for Each 5-ns Run[b]

run	E_{int} (SD) DOPC CHOL	E_{int} (SD) DOPC GLY	E_{int} (SD) DOPC double bond	E_{int} (SD) DOPC terminal CH_3
1	−1.08 (0.11)	−0.734 (0.088)	−0.084 (0.053)	−0.026 (0.017)
2	−1.05 (0.29)	−0.758 (0.125)	−0.175 (0.102)	−0.047 (0.033)

[a] See Chart 1 for numbering system. [b] Standard deviations are given in parentheses.

To further assess the strength of the interactions of the $C_{2'}$ methylene group (see labeling in Chart 1; this is the methylene group contained in the $-CH_2OH$ headgroup) with the different DOPC components, we computed the van der Waals interaction energy of this group with various lipid functional groups. Because these interaction energies decrease rapidly with distance ($\sim 1/r^6$), as the interaction energy increases, the groups under consideration become closer. These results are given in Table 1 for the two 5-ns trajectories. Each trajectory was split into five 1-ns sections, and the average energies were calculated over each nanosecond. The results for these five 1-ns sections were then averaged, and standard deviations were computed. Here, the standard deviations are given in parentheses after the interaction energy. It is clear in Table 1 that the strongest interaction of the headgroup $C_{2'}$ methylene of **1** is with the DOPC choline (CHOL) group followed closely by the interaction with the glycerol (GLY) group. The weakest interaction occurs with the terminal methyl groups of DOPC (terminal CH_3), which, as seen in Figure 2, have a distribution that peaks in the center of the bilayer. Thus, on average, the $-CH_2OH$ group of **1** and the DOPC terminal methyl groups are widely separated in the bilayer. This relatively large distance leads to the small interaction energy observed in Table 1. Finally, the interaction of the $C_{2'}$ methylene group with the DOPC double bonds is intermediate between the strong phospholipid headgroup interactions and the weaker terminal methyl interactions.

Figure 2b also shows the scaled group distributions for the hydrocarbon tail (terminal methyl) of **1** (shown in orange hatched region) and the terminal methyl region for DOPC (shown in red). Comparison with Figure 2a reveals that these terminal methyls exist in the hydrocarbon core region of DOPC (shown in purple in Figure 2a). It is clear here, then, that the terminal methyl of **1** is embedded in the DOPC hydrocarbon core chain region of the bilayer, with its maximum density at the bilayer center.

Hydrogen-Bonding Analysis. Intermolecular Hydrogen Bonding. We determined the presence and/or frequency of hydrogen-bonding patterns, both inter- and intramolecular, from the MD trajectories. In Table 2, we report the complete hydrogen-bonding analysis for the headgroup hydroxyl and amide NH group of **1**. To assess intermolecular hydrogen bonding, trajectories were analyzed for hydrogen bonding between the −OH or −NH of **1** and the DOPC phosphate, DOPC ester, or water via the H-bond analysis facility of CHARMM.[26] The hydrogen bonds counted for water (or the phosphate

Table 2. Average Percentage Lifetimes over a 10-ns MD Trajectory for the Various Hydrogen Bonds between DOPC Bilayer Constituents and the Headgroup Moieties of **1**[a]

bilayer constituent	$-CH_2OH$ average percentage time H-bond formed (%)	amide −NH average percentage time H-bond formed (%)
water[b]	66.2	69.0
DOPC (phosphate)	22.9	2.7
DOPC (ester)	4.5	14.2
no bilayer constituent	6.4	14.1[c]

[a] The H-bond facility of CHARMM (ref 26) was used for this analysis. [b] Water molecules that have penetrated into the phospholipid headgroup region (see Figure 2a). [c] Intramolecular hydrogen bonding accounted for 5.1%.

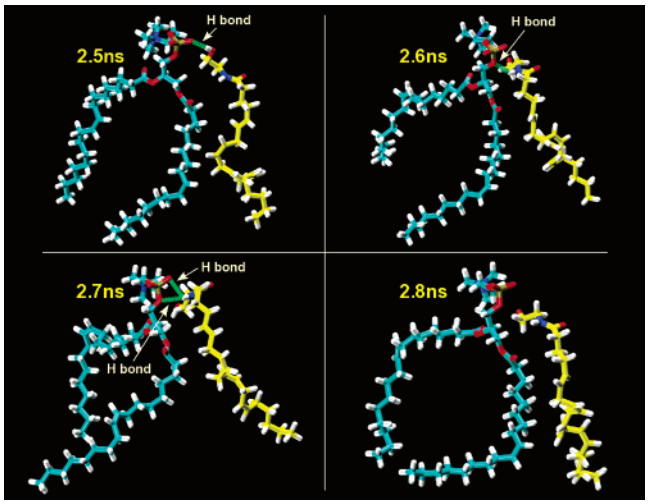

Figure 3. Time evolution of hydrogen bonding between **1** (carbons shown in yellow) and a DOPC phosphate group. The carbon atoms of DOPC are colored cyan. At 2.5 ns, the headgroup −OH of **1** forms a hydrogen bond with a DOPC phosphate oxygen. One-tenth of a nanosecond later (2.6 ns), the amide −NH of **1** forms a hydrogen bond with another DOPC phosphate oxygen. At 2.7 ns, the amide −NH of **1** forms a three-centered hydrogen bond with two phosphate oxygens of DOPC. One nanosecond later (2.8 ns), there is no hydrogen bond between **1** and DOPC.

or ester group) were not necessarily assigned to a specific molecule. These values represent the percentage of the simulation in which a certain type of hydrogen bond is present, rather than a specific, long-lived interaction. We observed in our simulations that hydrogen bonding between the hydrated DOPC bilayer and the headgroup of **1**, although extensive, was quite short-lived. It is clear from Table 2 that for the majority of simulation time (66.2% for −OH and 69.0% for −NH), the headgroup of **1** interacts with various water molecules that have penetrated the phospholipid headgroup region.[25] For **1**/DOPC hydrogen bonds, the −OH of **1** favored interactions with the DOPC phosphate group (22.9%), whereas the −NH of **1** favored hydrogen bonding with the DOPC ester group (14.2%). Over the two 5-ns trajectories, hydrogen bonds with the DOPC ester groups were found with the sn-2 chain ester moiety (67%) more frequently than they were found with the sn-1 chain ester moiety (33%). A typical example of the hydrogen-bond fluctuations seen during the simulations is provided in Figure 3, in which the selected frames are from 2.5 ns into the simulation to 2.8 ns (taken at 0.1 ns intervals) and **1** is colored yellow. At 2.5 ns, the −OH group of **1** forms a hydrogen bond with a DOPC phosphate oxygen. One-tenth of a nanosecond later (2.6 ns), the −NH group of **1** forms a hydrogen bond with another DOPC phosphate oxygen. At 2.7 ns, the −NH of **1** forms a three-centered hydrogen bond with two phosphate oxygens of DOPC. One nanosecond later (2.8 ns), there is no hydrogen bond between **1** and DOPC.

Intramolecular Hydrogen Bonding. The H-bond analysis facility of CHARMM[26] was also used to analyze the trajectories for the incidence of intramolecular hydrogen bonding in **1**. Two of the four molecules of **1** in the MD simulations were built with intramolecular hydrogen bonds between the amide oxygen and the hydroxyl hydrogen. These hydrogen bonds remained intact through the minimizaion of the system but were broken after heating and equilibration. This behavior is likely typical for this simulation procedure. However, no subsequent intramolecular hydrogen bonding between the amide oxygen and the hydroxyl group of **1** was observed in either of the two 5-ns trajectories. Our analysis did reveal the occasional presence of a hydrogen bond between the amide NH and the hydroxyl oxygen of **1**, however, with an average percentage lifetime of 5.1% over the two combined 5-ns trajectories.

Conformational Analysis of 1 in DOPC. Characterization of the conformational states of polyunsaturated fatty acids (PUFA) typically utilizes the torsion angle conventions defined in the work of Applegate and Glomset.[27] On the basis of this earlier work, Huber and co-workers,[28] Saiz and Klein,[25] and Gawrisch and co-workers[29] employed the following definitions for the vinyl methylene carbon dihedral angles (ωs), dihedrals that occur between two cis double bonds in the PUFA acyl chain. Referring to the carbon numbering for **1** in Chart 1, the $C_5-C_6-C_7-C_8/C_6-C_7-C_8-C_9$ dihedrals would be an example of an ($\omega 1$ $\omega 2$) pair. We have previously reported that such dihedral angles in **1** have maxima at +120° (labeled skew+) and at −120° (labeled skew−).[15] In the PUFA MD analysis of Huber and co-workers, [28] dihedrals with angles from 0 to 180° are denoted skew+ (or +), and those from 180 to 360° are denoted skew− (or −). The geometry about a given vinyl methylene group can be designated by the omega pairs ($\omega 1$ $\omega 2$), in which, for example, (± ±) indicates the case in which both $\omega 1$ and $\omega 2$ have the same sign (either + or −). We adopt a similar torsion angle representation here. The shape of the acyl chain is then primarily described by the sequence of these signs. For example, when the sequence ($\omega 1$ $\omega 2$) has the same sign, either (+ +) or (− −), that region of the acyl chain tends to adopt an elongated local conformation, whereas when the signs are opposite, a bending/kinking is introduced into the acyl chain. Compound **1** has three vinyl methylene carbons between cis double bonds, resulting in six dihedral angles that are necessary to simultaneously characterize the shape of the acyl chain through the unsaturated region. Following Applegate and Glomset,[27] we have denoted the following shapes: helical as (± ±)(± ±)(± ±); angle-iron as (± ±)(∓ ∓)(± ±); extended (e.g., combinations of helical/angle-iron) as (± ±)(± ±)(∓ ∓); hairpin as the (± ∓)(∓ ±) pattern at consecutive methylenes, and bent as the (± ∓) pattern at multiple (not consecutive) methylenes.

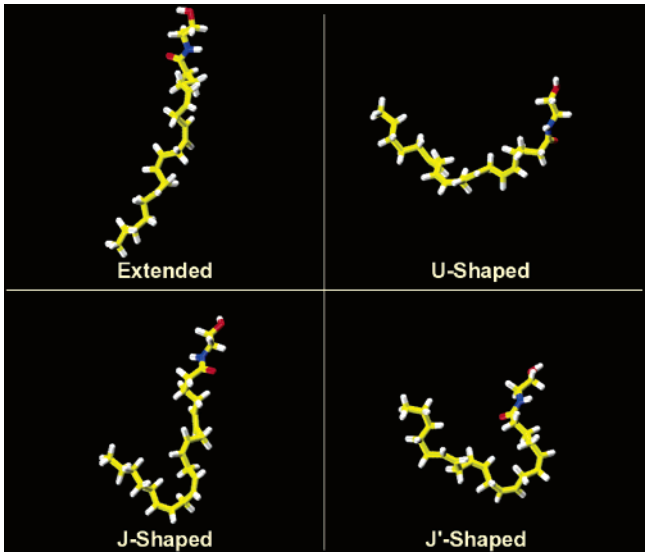

Figure 4. Representative conformations of **1** in DOPC: (top, left) an extended conformer (the extended structure category includes angle-iron and helical conformers); (top, right) a broad U-shaped conformer; (bottom, left) a J conformer, for which the short part of the J is near the end of the acyl chain of **1**; (bottom, right) a J′ conformer, for which the short part of the J is nearer the headgroup of **1**.

Unique structures have also been identified by Barnett-Norris and co-workers,[15,16] which are subsets of the bent shapes denoted by Applegate and Glomset. Those labeled "U" tend to have curvature at the first and third methylene carbons in the acyl chain of **1** but have an extended conformation at the middle or 2nd methylene carbon. These have a sign sequence of (± ∓)(± ±)(± ∓) (see Figure 2 in ref 15). In addition, an extended "U" with a sequence of (± ±)(± ∓)(± ±) has also been identified. Finally, a J-shaped structure has been identified as a low-energy structure for arachidonic acid on the basis of the MD simulations of Rich[30] and for **1** in the constrained MD simulations by Thomas and co-workers.[13] These structures are also subsets of the bent conformation discussed above, wherein a bend occurs at the end of the acyl chain nearer the polar headgroup such that a loop forms (see Figure 2 in ref 15), and the sign sequence for these structures is (± ∓)(± ±)(± ±). These structures are labeled J′ here. A second independent J-shaped (labeled J here) structure has been discussed by Barnett-Norris[15] with the "hook" nearer the terminal methyl group of the acyl tail and has a sign sequence of (± ±)(± ±)(± ∓). In Figure 4, several of these conformers are illustrated.

For **1**, with four double bonds and three vinyl methylene carbons, the full conformational mapping produces $2^6 = 64$ permutations of the methylene dihedrals of which half are mirror images. We have analyzed the entire 10 ns of the MD trajectories on the basis of these dihedral definitions and find that all 64 permutations are observed. Taking into account the mirror images, there are 32 unique conformations about the three vinylmethylene carbons in **1**. In Table 3, the distribution of these dihedrals is summarized, after taking into account their mirror images (the given conformation is placed into the population of its mirror image), and the percentages for those conformations that comprise a population that is 2% or greater are reported. Defining

Table 3. Percentage Population over a 10-ns Trajectory for the Various Acyl Chain Conformational States of **1**[a]

conformations	percentage (%)[b]
extended/helical/angle-iron	43.4
J[c]	15.6
J′[d]	10.7
U/extended U	20.7

[a] Shapes are illustrated in Figure 4. [b] The remaining 9.6% of the structures had random shapes. [c] Curvature in acyl tail region. [d] Curvature nearer headgroup region.

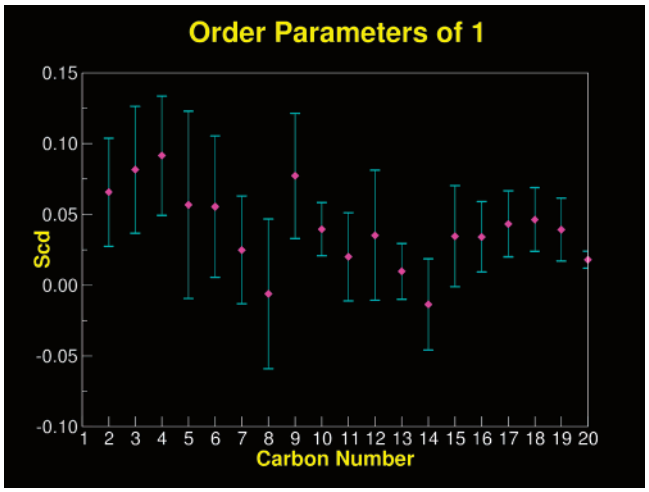

Figure 5. Calculated bond order parameters (S_{CD}, see eq 1) for the acyl chain of **1** in a model DOPC lipid bilayer. The carbon numbers on the *x*-axis refer to the carbon atoms in the arachidonoyl (acyl chain) portion of **1**. Error bars represent the 95% confidence intervals.

elongated conformations as those that are either helical, angle-iron, or extended, we find that 43.4% of the **1** molecules are in an elongated state, while 20.7% are in the U/extended U shape; 15.6% are in the J shape, and 10.7% are in the J′ shape.

Bond Order Parameters for 1 in DOPC. The average structure of the acyl chain segments of phospholipid bilayers can be characterized with the orientational bond order parameter. C−H bond order parameters are obtained experimentally by either deuterium substitution NMR, ^{2}H NMR, or ^{13}C NMR spectroscopies.[31,32] These order parameters may be expressed and computed from a MD trajectory using the following expression:[25,31]

$$S_{CD} = 1/2 \langle 3 \cos^2 \theta - 1 \rangle \qquad (1)$$

in which θ is the angle between the C−H bond vector and the normal to the bilayer surface, and the brackets indicate averaging over time (in a trajectory) and the number of molecules in the system.

In Figure 5, we report the C−H bond order parameters calculated from our MD trajectories for **1** in DOPC. As discussed by Grossfield and Woolf, [33] as well as by Eldho and co-workers,[32] it takes a relatively long simulation time to adequately converge these order parameters. Therefore, considering the length of the simulations reported here (10 ns total for four molecules of **1**), our purpose in presenting these data is to indicate *qualitative* trends in the data. The carbon numbers on the *x*-axis in Figure 5 refer to the carbon atoms in the arachidonoyl (acyl chain) portion of **1**. The magnitude

of the order parameters in Figure 5 is similar to that of the order parameters reported by Feller and co-workers for the polyunsaturated docosahexaenoic acid (DHA) chain in SDPC.[31] These order parameters are smaller than those typically seen for saturated lipid fatty acid chains (see Figure 6 in ref 31). In addition, the order parameters reported for **1** in Figure 5 are smaller for carbons closer to the bilayer center (i.e., carbons near the end of the acyl chain of **1**) than for those closer to the phospholipid headgroup/glycerol region (i.e., acyl chain carbons near the headgroup of **1**). Thus, there is a decrease in the order going from the water/lipid interface toward the center of the bilayer (i.e., C_1 to C_{20}). The error bars on the calculated data in Figure 5 represent the 95% confidence intervals and are reasonably large. However, a Student *t*-test indicates that the order parameters for the C_2, C_3, and C_4 atoms (see structure insert in Figure 5) are significantly different ($p < 0.05$) from those closer to the bilayer center ($C_{10}-C_{20}$).

Discussion

Water Penetration into the DOPC Bilayer. Figure 2a illustrates that in our simulations, water penetrates the polar headgroup region of the DOPC bilayer. The extent of water penetration into a fluid DOPC bilayer has been demonstrated in the joint X-ray and neutron diffraction studies of Wiener and White.[22] Their analysis highlights the dynamic nature of a lipid bilayer in the fluid phase, wherein the atomic locations of the various chemical components are described by distributions that overlap to varying degrees. For example, the distribution of water is seen to overlap significantly with the choline, phosphate, glycerol, and ester regions (see Figure 4 in ref 22). It is important to note that these diffraction experiments were run at very low hydration. The effect of hydration on water penetration has been studied by Simon and McIntosh[34] via X-ray diffraction and specific capacitance measurements on phosphatidylethanolamine. These studies showed that water penetrates the ester carbonyl regions of the phospholipid. Moreover, water contact with these ester carbonyls has also been observed via FT-IR spectroscopy of ^{13}C-labeled C=O groups in various phospholipids.[35] In general, water penetration is limited to the extent of the carbonyl region of the ester group; that is, *most* water molecules do not penetrate further into the hydrophobic core of the bilayer than do these carbonyl groups. This is in good agreement with our present results as well as with earlier high-hydration simulations of DOPC and 1-palmitoyl-2-oleoyl-*sn*-glycero-3-phosphocholine (POPC). [21]

Although most water molecules are limited to regions of the phospholipid bilayer up to the carbonyl groups, the combined X-ray and neutron diffraction results[22] indicate that there is a small overlap of water with the carbon−carbon double bonds of the DOPC acyl chains, suggesting short-lived excursions of water molecules occuring reasonably deep in the acyl chain region of the bilayer. It has been proposed that these excursions are the mechanism for the transport of permeants across the hydrophobic core of the bilayer. As seen in Figure 2a, our results indicate that although the water density is effectively zero at the center of the bilayer, there is some small overlap of the terminal methyl groups of the DOPC molecules with water. Moreover, this penetration seems to be slightly deeper in DOPC than in POPC, [21] an effect that likely results from the larger area per lipid in DOPC that would allow relatively more water molecules to intrude further into the headgroup region.

Location of 1 in DOPC. As seen in Figure 2b, the $-CH_2OH$ portion of the headgroup of **1** (yellow scored region) overlaps the glycerol (green) and choline (cyan) moieties of the DOPC phospholipid bilayer, being centered on the glycerol group. From Table 1, it is clear that the strongest interaction of the headgroup $C_{2'}$ methylene group of **1** is with the choline group, followed closely by the interaction with the glycerol, and then the interaction with the double bond and terminal methyl groups of DOPC. These results indicate that, on average, the $-CH_2OH$ moiety of the polar headgroup of **1** in DOPC resides in the phospholipid headgroup region of the DOPC bilayer.

Similarly, the group distributions for the hydrocarbon tail of **1** (shown as the orange hatched region, Figure 2b) indicate that the tail of **1** is embedded in the hydrocarbon core (shown in purple in Figure 2a) region of the bilayer with the maximum density for the terminal methyl of **1** (like that for the terminal methyl of DOPC in red) at the bilayer center. Taken together, these results suggest that, on average, the headgroup of **1** is located in the polar interface region (choline, glycerol region) of the DOPC bilayer, whereas the acyl chain of **1** extends into the hydrophobic core of the bilayer. In this way, the environments for the polar headgroup and nonpolar acyl chain of **1** are satisfied. Similar results have been obtained via MD studies for the free energy profile of valproic acid.[36] Valproic acid, $(CH_3CH_2CH_2)_2CH(COOH)$, is a small, amphiphilic, branched fatty acid with a polar carboxylic acid group and two short alkyl chains. In the studies of Ulander and Haymet,[36] the free energy minima for the translocation of valproic acid across a 1,2-dipalmitoyl-*sn*-glycero-3-phosphocholine (DPPC) bilayer occurs near the interface of the polar headgroup and alkyl chain region of the phospholipid bilayer, suggesting that this amphipathic fatty acid prefers to place its polar carboxylic acid group in the polar headgroup region of DPPC and its alkyl chains in the alkyl chain region of DPPC.

NMR cross-relaxation rates of magnetization transfer have been reported for **1** at 50 mol % in 1-stearoyl-2-oleoyl-*sn*-glycero-3-phosphocholine (SOPC) (Gawrisch, K. NIAAA, Bethesda, MD. Personal communication, 2005; ref 24). The results of these experiments indicated that the cross-relaxation rates for the headgroup $C_{2'}$ carbon of **1** (see Chart 1) with the lipid are largest for the choline and glycerol components and quite small for the SOPC terminal methyl group. Large cross-relaxation rates are indicative of close proximity; therefore, these results indicate that the headgroup of **1** is located in the lipid−water interface (i.e., the DOPC polar headgroup region), which is in agreement with the simulation results reported here.

Hydrogen-Bonding Patterns. Solid-state NMR measurements for **1** at 50 mol % in an SOPC lipid matrix have indicated that hydrogen bonding between the amide of **1** and an SOPC phosphate group is short-lived

(Gawrisch, K. NIAAA, Bethesda, MD. Personal communication, 2005; ref 24). As illustrated in Figure 3, typical hydrogen bonds between the amide −NH group of **1** and the DOPC phosphate group form and are broken within 0.2 ns. Although such hydrogen bonding is widespread, no individual hydrogen bond lasts longer than ∼0.25 ns. These results, therefore, agree with the NMR data from the Gawrisch lab.

Intramolecular hydrogen bonding between the amide oxygen and the hydroxyl group of **1**, which has been identified via MC simulations in DMSO[17] and suggested in the NMR studies of Eldho and co-workers,[24] are not observed in our simulation. Apparently, at the low concentration of **1** we have employed (∼5%), the competition with water and phospholipid components is sufficiently strong that this intramolecular hydrogen bonding is not significant. Our calculations indicate only a relatively weak and infrequent (5.1%) occurrence of intramolecular hydrogen bonding between the amide −NH and the hydroxyl oxygen of **1**.

Conformational Preferences of 1 in DOPC. Our MD simulations in DOPC have shown that many different conformations of **1** are possible in DOPC (Table 3). These include helical/angle-iron/extended, U/extended U, J, and J′ conformations. Figure 4 illustrates each of these conformations. The extreme conformational flexibility of **1** evident in Table 3 and Figure 4 is largely due to the low torsional energy barrier for rotation about the Csp^2-Csp^3 bonds in the acyl chain of **1**. This low torsional energy barrier was first described by Rich in MD studies of arachidonic acid in vacuo[30] and was recently quantified using ab initio quantum chemistry by Feller and co-workers.[31] Molecular simulations for other PUFAs, including docosahexaenoic acid (DHA),[27,37] and for PUFAs incorporated into lipid, including SDPC and 1-palmitoyl-2-docosahexaenoyl-*sn*-glycero-3-phosphocholine (PDPC), [25,28,29,31] have characterized the effects of the low torsional energy barrier for rotation about the Csp^2-Csp^3 bonds. Huber and co-workers[28] noted that the DHA chain in PDPC samples all possible conformational states about the five methylene linkers in the PUFA chain in a 6.0-ns simulation. Analogous conclusions have been reached by Saiz and Klein for SDPC.[25] Our results are in agreement with the results reported in the earlier studies of PDPC and SDPC, which show that the acyl chain of PUFAs adopts a large number of energetically accessible conformations, ranging from extended (helical/angle-iron), to more compact (U/hairpin-shaped), to folded (J-shaped) conformations.

Makriyannis and co-workers recently reported an NMR conformational study of two classical cannabinoids, Δ^8-THC and Me-Δ^8-THC, in phospholipid bicelles employed as a membrane bilayer model.[38] These investigators documented conformational differences between these two ligands that were a reflection of the conditions imposed by the bilayer-like environment on each ligand. Previous experimental and theoretical studies of **1** in other environments have illustrated the existence of great conformational flexibility and have also illustrated the importance of the environment in influencing the distribution of the observed conformations of **1**. For example, earlier MC (conformational memories) studies of **1** reported by our laboratory in an implicit $CHCl_3$ solvent model showed that extended conformations of **1** constituted approximately 28% of the total conformations,[15] and 23% were extended U-shaped conformations. In a high dielectric (water) solvent model, the predominant conformation (73%) of **1** was found by conformational memories to be a hybrid shape that was somewhere between an extended and a U shape. NMR experimental results for **1** in DMSO combined with the constrained/vacuum MC simulations reported by Bonechi and co-workers suggest a flexible acyl chain that primarily adopts a hybrid extended/U-shaped conformation.[17] MD results reported here for **1** in DOPC suggest that the environment of the DOPC phospholipid bilayer model more strongly favors elongated conformations of **1** (43.4%), with U-shaped (20.7%) and J- (15.6%)/ J′- (10.7%) shaped conformations having smaller populations. Taken together, these studies suggest that environment clearly influences the prevalent conformations of **1**.

Our simulations have indicated that for **1** in DOPC, a J-shaped (J) conformation in which the curvature is at the hydrocarbon tail end is possible (see Figure 4 for an example). The J shape represents 15.6% of the population of **1** seen in the MD simulations reported here. On the basis of an early paper of Corey and co-workers[39,40]concerning arachidonic acid, Thomas proposed that a low-energy J-shaped conformation (here, called J′) in which the curving is near the ethanolamide end of **1** may be the bioactive conformation of **1**.[13] The J′ shape conformation (± ∓)(± ±)(± ±) with the bend at the headgroup comprised a small, but nonnegligible population (∼3%) of our earlier MC-based simulations[15] and constitutes 10.7% of the population from MD results reported here (Table 3).

In the J conformation (± ±)(± ±)(± ∓) defined above and pictured in Figure 4, the bend is in the acyl tail portion of **1**. Since this tail is located toward the center of the bilayer (on average, see Figure 2b), which is a less dense region of the bilayer compared to the phospholipid headgroup region, it is likely that it is easier to form J conformations in the bilayer. This may contribute to the higher incidence (15.6%) of the J shape reported here. When **1** adopts the J′ shape, its polar headgroup is located in the phospholipid headgroup region, and the curved portion of the J′ conformation must be accommodated in/near the relatively dense headgroup region of the phospholipid bilayer. This may contribute to the lower probability (10.7%) of this conformation in the chemically heterogeneous environment of a phospholipid bilayer.

Order Parameters. Recent MD simulations and NMR measurements of SDPC[31,32] and PDPC[28] indicate low-energy barriers (∼1 kcal/mol) for rotation about the methylene single bonds located between the carbon−carbon cis double bonds in the sn-2 polyunsaturated chain, confirming the earlier modeling results for this barrier by Rich for arachidonic acid.[30] In experimental and MD studies of the structure of phospholipid bilayers, it has been shown that acyl chains that are polyunsaturated (typically the sn-2 chain) have dramatically lower bond order parameters than do those chains that are saturated (typically the sn-1 chain).[25,31] The results illustrated in Figure 5 indicate that the magnitude of the order parameters for **1** is similar to

that of the order parameters reported by Feller and co-workers for the polyunsaturated DHA chain in SDPC.[31] These order parameters are smaller than those typically seen for saturated lipid fatty acid chains (see Figure 6 in ref 31). As discussed by Feller and co-workers[31] and Huber and co-workers,[28] the origin of such small order parameters for polyunsaturated acyl chains can be a result of either (1) a conformational preference for a geometry wherein the angle between the C−H bond vector and the *z*-direction (normal to the surface of the membrane) is close to the magic angle value (54.7°) or (2) the fact that, over time, there are extensive fluctuations in the orientation of this CH bond vector. In the former case, the order parameter is small due to a rigid alignment of the C−H vectors with the bilayer normal such that the magic angle is achieved, whereas, in the latter case, the small value results from averaging the fluctuating values of the orientation of the C−H bond vector. Feller and co-workers [31] have shown that the θ probability distribution is nearly uniform for the C−H vector in DHA (see Figure 7 in ref 31), indicating essentially complete conformational sampling of the bond vectors with respect to the bilayer normal, rather than a rigid orientation locked in the magic angle (θ = 54.7°). Combined with NMR relaxation times, these results suggest that the acyl chains in polyunsaturated fatty acids have extensive conformational freedom, undergo rapid interconversion about the flexible methylene linkers, and access a large number of configurations. Therefore, the low bond order parameters for **1** reported in Figure 5 can be interpreted as an indication that the acyl chain of **1** in DOPC also has extensive conformational freedom, and the conformational analysis results for **1** (Table 3 and Figure 4) reported here are very consistent with this interpretation.

Implications for Endocannabinoid/Protein Interactions. The observation of rapidly forming/breaking hydrogen bonding for **1** with various lipid components identified in the simulations reported here, combined with the observation from our simulations (data not shown) that **1** and DOPC move laterally at a similar rate, suggests that **1** is mobile in the bilayer and capable of diffusing to membrane-embedded targets such as the CB1 receptor and FAAH. The result that **1** has high flexibility in the DOPC model bilayer but is, on average, elongated in the membrane, with its alkyl tail near the bilayer center, may have implications for interactions between **1** and its membrane-embedded/associated protein targets. In previous work in a model system, we have shown that the agonist alkyl tail interaction with the CB1 V6.43/I6.46 groove on TMH6 induces an activated state conformation in TMH6.[41] In the full receptor in its inactive state, this V6.43/I6.46 groove is located on the TMH6 lipid face of CB1. It is interesting that the elongated conformation of **1** in the DOPC bilayer places the alkyl tail of **1** in the same region of the bilayer as the V6.43/I6.46 groove (i.e., near the bilayer center). Studies are currently under way in our laboratory to determine whether, in a bilayer environment, **1** can interact with this groove and whether this interaction can induce an activated state conformation in TMH6.

Conclusions

In the present study, the structural and dynamical characteristics of **1** at a low concentration (∼5 mol %) in a DOPC lipid bilayer are investigated. The hydrogen-bonding analysis reported here suggests that although hydrogen bonding is extensive for **1** in lipids, there are no *long-lived* **1**−DOPC hydrogen bonds. In addition, intramolecular hydrogen bonds in **1** are only observed infrequently. This is likely because the competition with water and phospholipid components is sufficiently strong to favor intermolecular hydrogen bonding. Conformational analysis of our combined 10-ns MD trajectory indicates that **1** assumes all possible conformations in the lipid bilayer. Calculated order parameters are consistent with this, indicating great flexibility in the acyl chain of **1**. However, in contrast to our earlier solution phase studies,[15,16] we find that an extended conformation of **1** is favored in the chemically heterogeneous phospholipid bilayer. Scaled group distributions suggest that the polar headgroup of **1** resides, on average, at the lipid/water interface (i.e., the DOPC polar headgroup region), and the acyl chain of **1** resides in the hydrophobic core region of the bilayer with the terminal methyl near the bilayer center. The orientation of **1** produced by the lipid bilayer may prepare **1** for productive interaction with membrane-embedded proteins such as the cannabinoid CB1 receptor and with membrane-associated proteins such as FAAH, the enzyme that degrades **1**.

Methods

The two 5-ns simulations reported here employed the NAMD2 [42] molecular dynamics software package with the CHARMM27 parameter set,[43−45] including data for polyunsaturated lipids,[31] along with the TIP3P model for water. Force field parameters for **1** were constructed by the use of existing parameters for similar atom types. For example, the polyunsaturated acyl chain parameters necessary for the hydrocarbon chain of **1** are included in the current lipid force field.[31] Amide and hydroxyl values were taken from the serine amino acid parameter set. Periodic boundary conditions were employed with the long-range Coulombic electrostatic potential treated with the particle mesh Ewald summation method,[46] and the Lennard−Jones potential was smoothly cut off between 8.5 and 10 Å. The NAMD2 simulations reported here used the r-RESPA multiple time step algorithm, with a time step of 4 fs for long-range electrostatic forces, 2 fs for short-range nonbonded forces, and 1 fs otherwise. In production runs, configurations were stored every 1 ps for later analysis. All simulations were run at 310 K, and this temperature was maintained using Langevin dynamics.

The initial configuration for **1** in DOPC (see chemical structures for **1** and DOPC in Chart 1) was constructed as follows: First, a high-hydration bilayer patch of DOPC (72 lipid molecules with 36 in each leaflet) was generated by taking a low-hydration sample[18] and adding enough water molecules to achieve full hydration (27.5 water molecules/lipid molecule). This system was energy minimized, heated to 310 K, and the dynamics were run for 2 ns. The area was held constant at 67.5 A^2/lipid molecule, a value from DOPC area per lipid calculations reported by Mashl and co-workers at various hydration levels (see Table 1 in ref 19), and was interpolated for the hydration level in the calculations reported here (27.5 water molecules per lipid).[19] Values for the membrane area set point were obtained by Mashl and co-workers from the area per lipid, A_L, estimated from a volumetric relationship [47] among the water volume, the lipid volume, and Bragg spacing: $A_L = 2(V_L + n_W V_W)/D$, in which V_L is the volume of a lipid molecule, V_W is the volume of a water molecule, n_W is

the number of waters per lipid, and D is the experimental X-ray Bragg spacing at various hydration levels for DOPC. [48]

The MD was run in an NPAT ensemble, which represents a simulation cell with a volume that may fluctuate via changes in the z-direction coordinate while the area per lipid is held constant. The pressure was maintained at 1 atm via the Langevin piston Nose−Hoover method,[49,50] using a piston temperature of 310 K and a damping time/period of 100/200 fs.

To improve statistics, four molecules of **1** were included in the high-hydration bilayer patch of DOPC employed in all runs reported here. This makes the effective concentration of **1** in the simulations ∼5 mol %. With the use of a snapshot from the pure DOPC simulation, two DOPC molecules were removed, one from each bilayer, and four molecules of **1** were inserted, two in each leaflet. In each leaflet, one of the molecules was positioned in the location where the DOPC was removed, and the second molecule was placed at a distance that was approximately one-half the size of the simulation box from the first. The placement of the four molecules of **1** was such that the distance between the molecules exceeded the 10-Å cutoff for the nonbonded, short-range interactions employed in the calculations. Consequently, the molecules of **1** were placed far enough apart from each other during the simulation so that each acted independently of the others. The simulation cell contained a total of 15 857 atoms. Two of the molecules of **1** were built with an intramolecular hydrogen bond between the amide oxygen and the hydroxyl hydrogen in the headgroup and were sufficiently buried in the DOPC headgroup region such that they were not within 5 Å of a water molecule.

Steric overlap between the initially placed molecules of **1** and the lipid/water molecules was relieved by allowing the latter to adiabatically relax in the presence of the molecules of **1**. This was achieved by freezing the positions of the atoms in **1** and replacing them with van der Waals spheres of very small radii and then minimizing the lipid and water molecules in the presence of these spheres. One hundred steps of minimization were performed. The radii of the spheres were slowly increased (in eight steps) with 100 steps of minimization performed during each step. In the final step, the spheres returned to the values used in the normal CHARMM force field for these types of atoms. At this point, a full minimization, using the CHARMM force field parameters for **1**, was performed. Similar approaches for slowly growing cholesterol in lipids have been reported.[51]

Subsequently, the system was heated in steps of 50 K from 0 to 310 K (physiological conditions) at a constant volume, using Langevin coupling to a heat bath,[52] with a distance restraint imposed on the intramolecular hydrogen bond in the headgroup of **1**. This restraint was released, and an additional 0.25 ns of heating was performed. The ensemble was switched to NPAT and equilibrated for an additional 2 ns, whereupon the damping parameters were reduced, and production runs were initiated. Two separate 5-ns NPAT trajectories were simulated for a total of 10 ns of simulation time. A snapshot of the simulation cell is illustrated in Figure 1. The H-bond analysis facility of CHARMM [26] was used to analyze the trajectories for the incidence of both inter- and intramolecular hydrogen bonding.

Acknowledgment. This work was supported by NIDA Grants DA03934 and DA000489 (P.H.R.), and supercomputing support was provided by the Pittsburgh Supercomputer Center, AAB Grant Nos. MCB030006P and MCB030017. This work was also supported by the Theoretical and Computational Biophysics Group, an NIH Resource for Macromolecular Modeling and Bioinformatics, at the Beckman Institute, University of Illinois at Urbana-Champaign, through the use of the software package NAMD2. Figures 1, 3, and 4 were made with VMD, which is owned by the Theoretical and Computational Biophysics Group. Finally, we would like to acknowledge helpful discussions with Dr. Klaus Gawrisch.

References

(1) Devane, W. A.; Hanus, L.; Breuer, A.; Pertwee, R. G.; Stevenson, L. A.; et al. Isolation and structure of a brain constituent that binds to the cannabinoid receptor. *Science* **1992**, *258*, 1946−1949.
(2) Mechoulam, R.; Ben-Shabat, S.; Hanus, L.; Ligumsky, M.; Kaminski, N. E.; et al. Identification of an endogenous 2-monoglyceride, present in canine gut, that binds to cannabinoid receptors. *Biochem. Pharmacol.* **1995**, *50*, 83−90.
(3) Hanus, L.; Abu-Lafi, S.; Fride, E.; Breuer, A.; Vogel, Z.; et al. 2-Arachidonyl glyceryl ether, an endogenous agonist of the cannabinoid CB1 receptor. *Proc. Natl. Acad. Sci. U.S.A.* **2001**, *98*, 3662−3665.
(4) Wilson, R. I.; Nicoll, R. A. Endocannabinoid signaling in the brain. *Science* **2002**, *296*, 678−682.
(5) Di Marzo, V.; Melck, D.; Bisogno, T.; De Petrocellis, L. Endocannabinoids: endogenous cannabinoid receptor ligands with neuromodulatory action. *Trends Neurosci.* **1998**, *21*, 521−528.
(6) Piomelli, D.; Beltramo, M.; Giuffrida, A.; Stella, N. Endogenous cannabinoid signaling. *Neurobiol. Dis.* **1998**, *5*, 462−473.
(7) Di Marzo, V.; Fontana, A.; Cadas, H.; Schinelli, S.; Cimino, G.; et al. Formation and inactivation of endogenous cannabinoid anandamide in central neurons. *Nature* **1994**, *372*, 686−691.
(8) Piomelli, D.; Beltramo, M.; Glasnapp, S.; Lin, S. Y.; Goutopoulos, A. et al. Structural determinants for recognition and translocation by the anandamide transporter. *Proc. Natl. Acad. Sci. U.S.A.* **1999**, *96*, 5802−5807.
(9) Fegley, D.; Kathuria, S.; Mercier, R.; Li, C.; Goutopoulos, A.; et al. Anandamide transport is independent of fatty-acid amide hydrolase activity and is blocked by the hydrolysis-resistant inhibitor AM1172. *Proc. Natl. Acad. Sci. U.S.A.* **2004**, *101*, 8756−8761.
(10) Glaser, S. T.; Abumrad, N. A.; Fatade, F.; Kaczocha, M.; Studholme, K. M.; et al. Evidence against the presence of an anandamide transporter. *Proc. Natl. Acad. Sci. U.S.A.* **2003**, *100*, 4269−4274.
(11) McFarland, M. J.; Porter, A. C.; Rakhshan, F. R.; Rawat, D. S.; Gibbs, R. A.; et al. A role for caveolae/lipid rafts in the uptake and recycling of the endogenous cannabinoid anandamide. *J. Biol. Chem.* **2004**, *279*, 41991−41997.
(12) Bracey, M. H.; Hanson, M. A.; Masuda, K. R.; Stevens, R. C.; Cravatt, B. F. Structural adaptations in a membrane enzyme that terminates endocannabinoid signaling. *Science* **2002**, *298*, 1793−1796.
(13) Thomas, B. F.; Adams, I. B.; Mascarella, S. W.; Martin, B. R.; Razdan, R. K. Structure−activity analysis of anandamide analogues: relationship to a cannabinoid pharmacophore. *J. Med. Chem.* **1996**, *39*, 471−479.
(14) Tong, W.; Collantes, E. R.; Welsh, W. J.; Berglund, B. A.; Howlett, A. C. Derivation of a pharmacophore model for anandamide using constrained conformational searching and comparative molecular field analysis. *J. Med. Chem.* **1998**, *41*, 4207−4215.
(15) Barnett-Norris, J.; Guarnieri, F.; Hurst, D. P.; Reggio, P. H. Exploration of biologically relevant conformations of anandamide, 2-arachidonylglycerol, and their analogues using conformational memories. *J. Med. Chem.* **1998**, *41*, 4861−4872.
(16) Barnett-Norris, J.; Hurst, D. P.; Lynch, D. L.; Guarnieri, F.; Makriyannis, A.; et al. Conformational memories and the endocannabinoid binding site at the cannabinoid CB1 receptor. *J. Med. Chem.* **2002**, *45*, 3649−3659.
(17) Bonechi, C.; Brizzi, A.; Brizzi, V.; Francoli, M.; Donati, A.; et al. Conformational analysis of N-arachidonylethanolamide (anandamide) using nuclear magnetic resonance and theoretical calculations. *Magn. Reson. Chem.* **2001**, *39*, 432−437.
(18) Feller, S. E.; Yin, D.; Pastor, R. W.; MacKerell, A. D., Jr. Molecular dynamics simulation of unsaturated lipid bilayers at low hydration: parametrization and comparison with diffraction studies. *Biophys. J.* **1997**, *73*, 2269−2279.
(19) Mashl, R. J.; Scott, H. L.; Subramaniam, S.; Jakobsson, E. Molecular simulation of dioleoylphosphatidylcholine lipid bilayers at differing levels of hydration. *Biophys. J.* **2001**, *81*, 3005−3015.
(20) Tristram-Nagle, S.; Petrache, H. I.; Nagle, J. F. Structure and interactions of fully hydrated dioleoylphosphatidylcholine bilayers. *Biophys. J.* **1998**, *75*, 917−925.
(21) Chiu, S. W.; Jakobsson, E.; Subramaniam, S.; Scott, H. L. Combined Monte Carlo and molecular dynamics simulation of fully hydrated dioleyl and palmitoyl-oleyl phosphatidylcholine lipid bilayers. *Biophys. J.* **1999**, *77*, 2462−2469.

(22) Wiener, M. C.; White, S. H. Structure of a fluid dioleoylphosphatidylcholine bilayer determined by joint refinement of X-ray and neutron diffraction data. III. Complete structure. *Biophys. J.* **1992**, *61*, 437−447.
(23) Chen, J. Z.; Han, X. W.; Xie, X. Q. Preferred conformations of endogenous cannabinoid ligand anandamide. *Life Sci.* **2005**, *76*, 2053−2069.
(24) Eldho, N. V.; Gawrisch, K. Location, conformation and dynamics of anandamide in biomembranes. *Biophys. J.* **2003**, *84*, 49a.
(25) Saiz, L.; Klein, M. L. Structural properties of a highly polyunsaturated lipid bilayer from molecular dynamics simulations. *Biophys. J.* **2001**, *81*, 204−216.
(26) Brooks, B. R.; Bruccoleri, R. E.; Olafson, B. D.; States, D. J.; Swaminathan, S.; et al. CHARMM: a program for macromolecular energy, minimization, and dynamics calculations. *J. Comput. Chem.* **1983**, *4*, 187−217.
(27) Applegate, K. R.; Glomset, J. A. Computer-based modeling of the conformation and packing properties of docosahexaenoic acid. *J. Lipid Res.* **1986**, *27*, 658−680.
(28) Huber, T.; Rajamoorthi, K.; Kurze, V. F.; Beyer, K.; Brown, M. F. Structure of docosahexaenoic acid-containing phospholipid bilayers as studied by (2)H NMR and molecular dynamics simulations. *J. Am. Chem. Soc.* **2002**, *124*, 298−309.
(29) Gawrisch, K.; Eldho, N. V.; Holte, L. L. The structure of docosahexaenoic acid in phospholipid membranes. *Lipids* **2003**, *38*, 445−452.
(30) Rich, M. R. Conformational analysis of arachidonic and related fatty acids using molecular dynamics simulations. *Biochim. Biophys. Acta* **1993**, *1178*, 87−96.
(31) Feller, S. E.; Gawrisch, K.; MacKerell, A. D., Jr. Polyunsaturated fatty acids in lipid bilayers: intrinsic and environmental contributions to their unique physical properties. *J. Am. Chem. Soc.* **2002**, *124*, 318−326.
(32) Eldho, N. V.; Feller, S. E.; Tristram-Nagle, S.; Polozov, I. V.; Gawrisch, K. Polyunsaturated docosahexaenoic vs docosapentaenoic acid-differences in lipid matrix properties from the loss of one double bond. *J. Am. Chem. Soc.* **2003**, *125*, 6409−6421.
(33) Grossfield, A. W.; Woolf, T. B. Interaction of tryptophan analogues with POPC lipid bilayers investigated by molecular dynamics calculations. *Langmuir* **2002**, *18*, 198−210.
(34) Simon, S. A.; McIntosh, T. J. Depth of water penetration into lipid bilayers. *Methods Enzymol.* **1986**, *127*, 511−521.
(35) Blume, A.; Hubner, W.; Messner, G. Fourier transform infrared spectroscopy of 13C = O-labeled phospholipids hydrogen bonding to carbonyl groups. *Biochemistry* **1988**, *27*, 8239−8249.
(36) Ulander, J.; Haymet, A. D. Permeation across hydrated DPPC lipid bilayers: simulation of the titrable amphiphilic drug valproic acid. *Biophys. J.* **2003**, *85*, 3475−3484.
(37) Rabinovich, A. L.; Ripatti, P. O. On the conformational, physical properties and function of polyunsaturated acyl chains. *Biochim. Biophys. Acta* **1991**, *1085*, 53−56.
(38) Guo, J.; Pavlopoulos, S.; Tian, X.; Lu, D.; Nikas, S. P.; et al. Conformational study of lipophilic ligands in phospholipid model membrane systems by solution NMR. *J. Med. Chem.* **2003**, *46*, 4838−4846.
(39) Corey, E. J.; Niwa, H.; Falck, J. R. Selective epoxidation of eicosa-*cis*-5,8,11,14-tetraenoic (arachidonic) acid and eicosa-*cis*-8,11,-14-trienoic acid. *J. Am. Chem. Soc.* **1979**, *101*, 1586−1587.
(40) Corey, E. J.; Iguchi, S.; Albright, J.; De, B. Studies on the conformational mobility of arachidonic acid. Facile macrolactonization of 20-hydroxyarachidonic acid. *Tetrahedron Lett.* **1983**, *24*, 37−40.
(41) Barnett-Norris, J.; Hurst, D. P.; Buehner, K.; Ballesteros, J. A.; Guarnieri, F.; et al. Agonist alkyl tail interaction with cannabinoid CB1 receptor V6.43/I6.46 groove induces a Helix 6 active conformation. *Int. J. Quantum Chem.* **2002**, *88*, 76−86.
(42) Kale, L.; Skeel, R.; Bhandaarkar, M.; Brunner, R.; Gursoy, A.; et al. NAMD2: greater scalability for parallel molecular dynamics. *J. Comput. Phys.* **1999**, *151*, 283−312.
(43) Schlenkrich, M.; Brickmann, J.; MacKerell, A. D., Jr.; Karplus, M. Empirical potential energy function of phospholipids: criteria for parameter optimization and applications. *Biological Membranes: A Molecular Perspective from Computation and Experiment*; Birkhauser: Boston, MA, 1996; pp 31−81.
(44) MacKerell, A. D., Jr.; Bashford, D.; Bellot, M.; Dunbrack, R. L., Jr.; Evanseck, J.; Field, M. J.; Fischer, S.; Gao, J.; Guo, H.; Ha, S.; Joseph, D.; Kuchnir, L.; Kuczera, K.; Lau, F. T. K.; Mattos, C.; Michnick, S.; Ngo, T.; Nguyen, D. T.; Prodhom, B.; Reiher, I. W. E.; Roux, B.; Schlenkrich, M.; Smith, J.; Stote, R.; Straub, J.; Watanabe, M.; Wiorkiewicz-Kuczera, J.; Yin, D.; Karplus, M. All-hydrogen empirical potential for molecular modeling and dynamics studies of proteins using the CHARMM22 force field. *J. Phys. Chem. B* **1998**, *102*, 3586−3616.
(45) Feller, S. E.; MacKerell, A. D., Jr. An improved empirical potential energy function for molecular simulations of phospholipids. *J. Phys. Chem. B* **2000**, *104*, 7510−7515.
(46) Darden, T. A.; York, D.; Pedersen, L. Particle mesh Ewald: an Nlog(N) method for Ewald sums in large systems. *J. Chem. Phys.* **1993**, *98*, 10089−10092.
(47) Nagle, J. F.; Wiener, M. C. Structure of fully hydrated bilayer dispersions. *Biochim. Biophys. Acta* **1988**, *942*, 1−10.
(48) Hristova, K.; White, S. H. Determination of the hydrocarbon core structure of fluid dioleoylphosphocholine (DOPC) bilayers by X-ray diffraction using specific bromination of the double-bonds: effect of hydration. *Biophys. J.* **1998**, *74*, 2419−2433.
(49) Feller, S.; Zhang, Y.; Pastor, R.; Brooks, B. Constant pressure MD simulations: the Langevin piston method. *J. Chem. Phys.* **1995**, *103*, 4613−4621.
(50) Martyna, G. L.; Tobias, D. J.; Klein, M. L. Constant pressure molecular dynamics algorithms. *J. Chem. Phys.* **1994**, *101*, 4177−4189.
(51) Hofsass, C.; Lindahl, E.; Edholm, O. Molecular dynamics simulations of phospholipid bilayers with cholesterol. *Biophys. J.* **2003**, *84*, 2192−2206.
(52) Bhandarkar, M.; Brunner, R.; Chipot, C.; Dalke, A.; Dixit, A.; et al. NAMD User's Guide, Version 2.5. University of Illinois and Beckman Institute, 2003.

JM058185D